Coexistence of trapped and free excess electrons in SrTiO$_3$

Xianfeng Hao,[1,2,3] Zhiming Wang,[1] Michael Schmid,[1] Ulrike Diebold,[1] and Cesare Franchini[2,*]

[1]*Institute of Applied Physics, Vienna University of Technology, Vienna, Austria*

[2]*University of Vienna, Faculty of Physics and Center for Computational Material Science, Vienna, Austria*

[3]*Key Laboratory of Applied Chemistry, Yanshan University, Qinhuangdao 066004, People's Republic of China*

The question whether excess electrons in SrTiO$_3$ form free or trapped carriers is a crucial aspect for the electronic properties of this important material. This fundamental ambiguity prevents a consistent interpretation of the puzzling experimental situation, where results support one or the other scenario depending on the type of experiment that is conducted. Using density functional theory with an on-site Coulomb interaction U, we show that excess electrons form small polarons if the density of electronic carriers is higher than $\approx 10^{20}$ cm^{-3}. Below this value, the electrons stay delocalized or become large polarons. For oxygen-deficient SrTiO$_3$, small polarons confined to Ti^{3+} sites are immobile at low temperature but can be thermally activated into a conductive state, which explains the metal-insulator transition observed experimentally.

I. INTRODUCTION

Strontium titanate is a key material in the emerging field of oxide electronics. It exhibits many attractive properties such as superconductivity [1], ferromagnetism [2,3], high thermoelectric coefficients [4], blue and green light emission [5], and can accommodate a two dimensional electron gas [6,7]. All these phenomena arise when a small number of electrons are introduced into the lattice. The characteristics and mobility of excess electrons is strongly determined by their interaction with the lattice through electron-phonon coupling. One of the manifestations of the electron-phonon interaction is the formation of a polaron, a quasiparticle formed by the excess electron and the structural deformations it induces [8,9]. Depending on the spatial extent of the polaronic wave function and associated structural distortions two types of polarons can be identified: in the small-polaron model the range of the distortion is of the order of the lattice constant, whereas in the large polaron the wave function spreads over several lattice sites and exhibits a more free-carrier-like behavior. Large polarons show a mobility inversely proportional to the number of longitudinal optical phonons. In contrast, small polarons form highly localized in-gap states and can hop to adjacent lattice sites when thermally activated [10].

Experimental information on the role of polarons in SrTiO$_3$ is abundant, yet controversial [11–24]. The key question is whether it is a large or a small polaron that is formed. Excess electrons introduced by doping or by oxygen defects have been identified as large polarons in transport measurements and optical spectroscopies [11,12]. The validity of this picture is supported by recent angle-resolved photoemission spectroscopy data [13]. Pump-probe spectroscopy in lightly photoexcited SrTiO$_3$ suggested that itinerant electron polarons are the origin of diffusive lattice distortions [14]. However, the large-polaron model cannot explain the in-gap bulk states in the conductive phase revealed in photoemission spectroscop [20–23]. Instead, these highly localized states are attributable to small polarons trapped in bulk sites. This interpretation is re-inforced by the recent observation that photoexcited electrons relax into self-trapped polaron states [14,18]. Electron trapping has been also invoked to explain the metal-insulator transition (MIT) in SrTiO$_{3-\delta}$ thin films [16] and single crystals [17]. To complicate the situation even further, there are indications that excess electrons localized in trapped states can coexist with free carriers [12,15,19,24]. No coherent picture can explain all these experiments so far; this has sparked an animated debate and poses a serious challenge to theory.

Computational studies provide additional insights. Based on density functional theory (DFT)+U, hybrid DFT, and model Hamiltonians, it was suggested that the two additional electrons donated by a single oxygen vacancy V$_O$ induce one singly occupied in-gap state mostly localized at the Ti atoms near the V$_O$, and one state delocalized in the conduction band [25–30]. This conclusion successfully clarifies transport and optical properties in reduced SrTiO$_3$, but is inconsistent with the observed V$_O$-induced MIT [16], because the predicted free carriers would be mobile even at low temperature.

The present study aims to provide a unified and coherent explanation of the role of excess electrons in SrTiO$_3$. In particular it investigates the conditions under which localized and free-electron-like states can form, coexist, and propagate. We show that a small-polaron regime is established if the carrier density n is higher than a critical value, both in the low-temperature antiferrodistortive (AFD) and in the cubic structure. Below this critical density, the excess electrons will be delocalized or form large polarons, leading to a metallic solution without in-gap states, in nice agreement with experiment. Moreover, we provide theoretical evidence that the two excess electrons donated by V$_O$ form two self-trapped electrons, which become mobile if thermally activated, thus supporting the temperature-driven MIT observed in reduced SrTiO$_3$ [16].

II. METHODS

For our calculations we adopted spin-polarized DFT+U within the gradient-corrected Perdew-Burke-Ernzerhof (PBE) functional [31] using the VASP [32]. An on-site U was applied to the d states of Ti. The value of the Coulomb and exchange

*cesare.franchini@univie.ac.at

parameters U and J was computed fully *ab initio* within the constrained random phase approximation [33]. To this aim the Kohn Sham orbitals were projected onto maximally localized Wannier functions [34] using the Wannier90 code [35,36]. For the construction of the correlated subspace we have followed the hybrid "d-dp Hamiltonian"-like approach suggested by Vaugier and co-workers [37], where the Wannier functions are generated for the metal d and oxygen p orbitals, and only the d bands are removed for the calculation of the effective interactions. Following this procedure we obtained $U = 4.96$ eV and $J = 0.51$ eV, and set $U - J = 4.5$ eV, which is in line with previous DFT+U studies of polarons in SrTiO$_3$ [25,27].

We considered both the cubic and the low-temperature (below 110 K) tetragonal AFD phase of SrTiO$_3$ and at the optimized lattice constants (a$_{cubic} = 3.948$ Å, a$_{AFD} = 3.937$ Å, and c/a$_{AFD}=1.0055$). Adopting these lattice constants the optmized rotation of the octahedra around the z axis in the AFD phase is about $6°$, in agreement with previous DFT-based calculations [38]. To mimic substitutional (Ti/Nb) doping and V$_{OS}$ we employed an $N \times N \times N$ supercell (SC) with $N = 3$, $4, 5$, and 6 (up to 1080 atoms). For each SC all atomic positions were relaxed until the residual force on each atom was less than 0.02 eV/Å.

The polaron formation energy is defined as the energy difference between the delocalized, free electron solution and the localized polaron solution. Both these solutions can be modeled by DFT. The delocalized solution can be achieved within a standard non-spin-polarized calculation. To model the small polaron solution different schemes can be adopted as recently discussed in Ref. [39]. We have followed the following strategy, proposed by Deskins *et al.* [40].

(1) First, we have chosen the specific Ti sites at which we aim to stabilize a polaron and substituted that distinct Ti with a V atom and let the structure relax within a spin-polarized setup. In this way we break the symmetry and allow an expansion of the oxygen octahedron around the V.

(2) Second, we placed back the Ti atom in the V position and let the structure relax within a spin-polarized setup by initializing a local magnetic moment equal to one in this specific Ti site.

For particularly complicated polaronic configurations (i.e., difficult to converge) we have added an intermediate step in which we have performed a step-(2) calculation using a larger value of the on-site U at the Ti site at which we wanted to form the polaron. In this way we could more easily attract the excess electron to that specific Ti site. In a subsequent run, we recovered the usual value of U and let the system relax. This procedure was repeated for several polaronic configurations and the corresponding total energies were compared to the total energy of the delocalized solution.

We verified that the results were converged with respect to the energy cutoff (400 eV) and number of k points (12 × 12 × 12 with respect to the primitive cubic cell). Molecular dynamics (MD) simulations of small polaron hopping in SrTiO$_{3-\delta}$ with $\delta \approx 0.00267$ were performed at simulated temperatures ranging from 700 K to 1000 K for 5 ps with a time step of 1 fs. The MD are also performed within the DFT+U framework. We expect that the inclusion of the intersite effective interaction V [41], which have never been employed to describe the dynamics of polarons, could improve

further the agreement with experiments. For SrTiO$_3$ our cRPA procedure delivers $V = 1.7$ eV.

III. RESULTS AND DISCUSSION

In this section we present and discuss the results obtained for the Nb-doping and oxygen vacancies calculations.

A. Nb doping

The substitution of one Ti with one Nb in a cubic $N = 3$ SC, corresponding to an electron density n of 6×10^{20} cm^{-3}, establishes a nonconducting state with a rather sharp peak at about 0.80 eV below the conduction band minimum (CBM, see Fig. 1), in line with the experimental values of 1.0–1.5 eV [18,20–23]. From an analysis of the charge character we infer that this state locates almost completely on one distinct Ti atom, and gives rise to a d^1_{xz} configuration with a magnetic moment of about $0.9\mu_B$. Consequently, the Ti atom is reduced to Ti^{3+}. The electron trapping is accompanied by local structural deformations manifested by the elongation of all Ti-O bond lengths within the Ti^{3+}O$_6$ octahedron by about

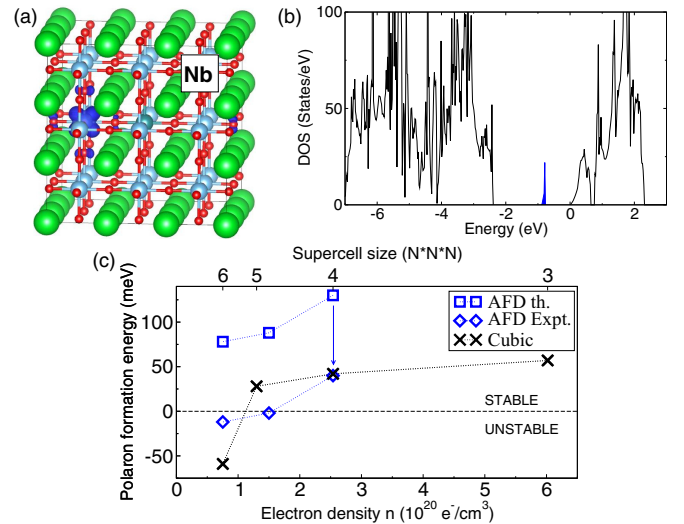FIG. 1. (Color online) Nb-doped SrTiO$_3$. (a) Isosurfaces of the spin density (dark blue; 0.045 e/Å) for an $N = 3$ supercell. The green (big), light-blue/turquoise (medium size), and red (small) balls represent Sr, Ti/Nb, and O atoms, respectively. (b) Electronic density of states ($N = 3$); the (blue) peak in the band gap corresponds to the polaron state formed at a Ti^{3+} site. (c) Variation of the polaron formation energy as a function of carrier density for the cubic ($N = 3$, 6.03×10^{20} cm^{-3}, 135 atoms; $N = 4$, 2.54×10^{20} cm^{-3}, 320 atoms; $N = 5$, 1.30×10^{20} cm^{-3}, 625 atoms; $N = 6$, 0.75×10^{20} cm^{-3}, 1080 atoms) and low-T AFD phases (2.54×10^{20} cm^{-3}, 320 atoms; 1.50×10^{20} cm^{-3}, 540 atoms; 0.75×10^{20} cm^{-3}, 1080 atoms) for the optimized (Theor.) and experimental (Expt.) volume. The AFD Expt. curves are obtained by shifting down the AFD Theor. curve by the calculated energy shift at $N = 4,90$ meV. For the 540 atoms AFD phase we adopted a supercell based on the a$_{AFD}\sqrt{2} \times$ a$_{AFD}\sqrt{2} \times$ c$_{AFD}$. The data are aligned with respect to the electron density (1 Nb per SC). Interpolating the polaron formation energy for $N \rightarrow \infty$ as a function of $1/N^3$ [42] confirms the delocalization solution in the dilute limit. The dotted line serves as a guide to the eye.
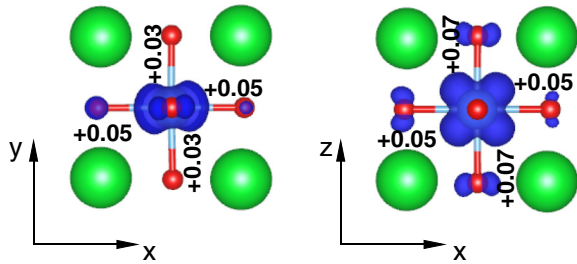
FIG. 2. (Color online) Local structural distortions of the Nb-induced polaron shown in Fig. 1(a) within the xy and xz planes. The numbers indicate the expansion (in Å) with respect to the ideal cubic Ti-O bond length.

0.05 Å as shown in Fig. 2. This is the typical fingerprint of a small polaron.

The stability of the small polaron is determined by the competition between the structural energy required to distort the lattice E_{ST}, and the electronic energy gained by localizing the excess electron at a specific Ti site E_{EL}. We found a positive polaron formation energy of 57 meV for the smallest $N = 3$ cubic supercell, which means that the small polaron is stable.

A key parameter, which has been largely overlooked in previous theoretical studies, is the role of the carrier density. To clarify this issue, we have performed analogous calculations using larger SCs, thus varying the doping concentration x from $x = 3.7\%$ ($N = 3, n = 6 \times 10^{20}$ cm^{-3}) to $x = 0.5\%$ ($N = 6$, $n = 7 \times 10^{19}$ cm^{-3}). We find that the polaron formation energy strongly depends on the carrier density; see Fig. 1(c). For the smallest Nb-doping SC ($N = 3$) we have also studied the effects of the change of the volume due to Nb doping. We found that the lattice constant expands from $a = 3.945$ Å to 3.993 Å and the polaron formation energy increases up to 140 meV. Following Vegard's law the volume expansion and its effect on the polaron formation energy becomes negligible for larger supercell for which the Nb concentration is very small.

Within the low-T AFD setup the small-polaron formation energy substantially increases for all values of the carrier density [Fig. 1(c), square symbols] using the optimized DFT+U volume. This is explained by the larger Ti-O bond lengths in the low-temperature AFD structure as well as its higher structural flexibility compared to the cubic phase; both make the small polaron more favorable. DFT-based calculations strongly overestimate the AFD distortions, however [38,43]. Therefore, more realistic values for the AFD phase will be closer to those for the cubic phase. Indeed, by performing AFD calculations for the $N = 4$ SC at the experimental lattice constants the polaron formation energy is reduced by about 90 meV as indicated in Fig. 1(c).

The stability of the small polaron decreases as the carrier density decreases. For $N \approx 6$ it eventually becomes negative, indicating that the excess electron is prone to delocalization over the entire SC, or to create a large polaron.

This localized-to-delocalized transition is explained by analyzing the energy balance involved in the electron trapping process. The small polaron is stable when the electronic energy gain $|E_{EL}|$ is larger than the structural energy loss $|E_{ST}|$. E_{ST} does not depend on the carrier density, but may depend

on the presence of the dopant (Nb). Indeed, we found that self-trapping in a perfect (defect free) lattice is unstable. An increased Ti^{3+}-O bond length for the O atom binding to a neighboring Nb dopant indicates that the dopant provides the crystal with the structural flexibility (i.e., small E_{ST}) needed to accommodate an electron in a locally distorted Ti^{3+} site close to the Nb impurity. This argument applies to other types of structural deformations such as surface reconstructions and steps, which are found to favor small polaron formation [44,45].

We have verified that the stability of a polaron decreases by increasing the Ti^{3+}-Nb distance and that the small polaron solution becomes unstable for Ti sites far from the Nb dopant. This indicates that dopants are necessary to activate electron trapping: without the dopant, excess electrons prefer to behave like free carriers. On the other hand, E_{EL} depends on the carrier density n through electronic correlation. The repulsion among the Nb-induced extra electrons is expected to get weaker at low concentration, attenuating the attraction between the excess electrons and the positively charged Nb center. Although small, this effect may become relevant for cases in which the polaron energy is very small ($E_{ST} \approx E_{EL}$).

To ascertain the role of U on the polaron formation energy we have also performed some calculations for different values
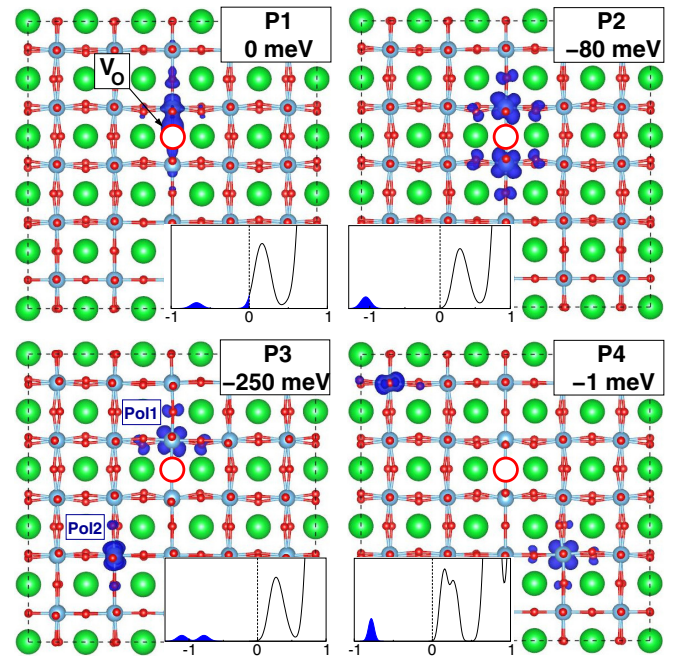

FIG. 3. (Color online) Isosurfaces of the spin density (0.045 e/Å^2) for one V$_O$ (circle) in an $N = 5$ SC. The insets show the density of states near the Fermi level (set at the CBM). The filled peaks indicate the polaron states. In the P1 polaron configuration, considered to be the ground state in previous computational studies [25–28], one electron is self-trapped near the V$_O$, while the other one is delocalized. For each polaronic configuration (P1–P4) the relative energy with respect to the P1 phase is given (in meV). The most stable polaron solution is P3. The two small polarons (high spin density) are labeled Pol1 and Pol2. A three dimensional view of the four polaron configurations is given in Fig. 4.

of U (± 1 eV with respect to the cRPA value). In agreement with previous studies we found that the polaron formation energy scales almost linearly with U [44]: for $N = 4$ the polaron formation energy becomes negative for $U - J = 4$ (cubic) and $U - J = 4.3$ (AFD).

Thus, in the limit of low concentration, E_{ST} becomes larger than E_{EL}, the polaron solution unstable, and the excess electron begins to delocalize. It is extremely challenging to accurately describe delocalized large polarons from first principles. By incorporating many-body effects in Fröhlich's large polaron Hamiltonian [8], Devreese *et al.* [12] have computed the low-T optical conductivity of Nb-doped SrTiO$_3$ with large polarons for different dopant concentrations and found the best agreement with experiment at low carrier concentration [$n = (1.7$–$3.4) \times 10^{19}$ cm^{-3}], in good agreement with the regime where we predict small polarons to be unstable [Fig. 1(c)]. Inserting the characteristic electron-phonon coupling constant [12] and the characteristic longitudinal optical phonon frequency [46] in Fröhlich's model, we obtain a spatial extension of the large polaron in SrTiO$_3$ of 9–19 Å, i.e., 3–5 unit cells.

Our findings resolve puzzling and apparently conflicting results observed in Nb-doped SrTiO$_3$. First, the unusually narrow Drude feature for carrier concentrations between 0.1% and 2% per unit cell [11] can be understood by the large-polaron model, in line with our calculations for a small carrier density. Second, the in-gap states detected by photoemission spectroscopy in moderately doped samples (1% < x < 5%) suggest a semiconducting regime [21], in excellent agreement with our small polaron picture. At the transition from localized to free-carrier behavior, where the formation energy of small polarons is very small, the thermal excitation is high enough to surmount it, resulting in a situation where the trapped and mobile electrons can coexist in the system. This picture can explain the existence of in-gap states in the conductive phase measured by photoemission spectroscopy studies [20–23], and can be rationalized in terms of an inhomogeneous distribution of impurities or defects as suggested in experimental works [47,48].

B. Oxygen vacancies

To analyze the reduced sample we employed a cubic $5 \times 5 \times 5$ SC with one V$_O$, resulting in two excess electrons per SC. Previous computational analyses suggest that one V$_O$ induces a singly occupied in-gap state, and donates one free carrier to the conduction band [25–28,30]. We label this mixed localized/free-carrier polaron configuration P1. The corresponding charge density isosurface is plotted in Fig. 3.

Based on a systematic search of several configurations we have identified three more stable polaron patterns (P2, P3, and P4; Fig. 3). All of them have an insulating density of states with polaron peaks between 0.8 and 1.1 eV below the CBM. The polaron topologies of the various configurations differ in distance between the polaron and the V$_O$, as depicted in Figs. 3 and 4. The most stable configuration is P3, with one polaron
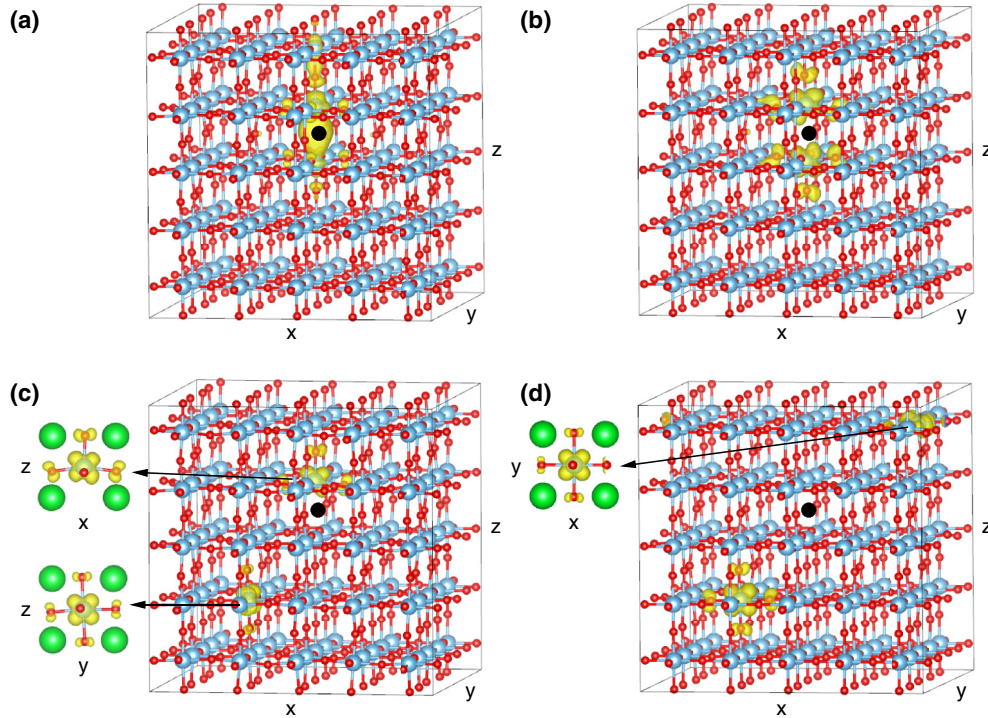

FIG. 4. (Color online) Three dimensional view of the four polaron configurations shown in Fig. 3 and corresponding spin density isosurfaces. Small (red) and large (blue) spheres represent oxygen and titanium atoms, respectively. Strontium atoms are not shown. The V$_O$ is indicated by a (black) filled circle. (a) P1: one electron is trapped near the V$_O$ in a d$_{z^2}$ orbital, while the second one is delocalized; (b) P2: both electrons are trapped near the V$_O$ in d$_{xz}$ orbitals; (c) P3: one electron is trapped near the V$_O$ in a d$_{xz}$ orbital, while the second one is located in a Ti^{3+} site ≈ 8 Å away with a d$_{yz}$ configuration (shown in the insets). (d) Both electrons are about 8 Å away from the V$_O$, and adopt d$_{xz}$ and d$_{xy}$ configurations.

anchored near V_O and the second one localized in a Ti^{3+} site ≈ 8 Å away from V_O. P3 is more favorable than P1 by 250 meV. Different from previous calculations, all our additional polaron states display a t_{2g} distribution instead of e_g (d_{z^2}).

From a structural point of view, removal of a single O atom makes the nearest-neighbor (NN) Ti (two) and Sr (four) atoms move away from the vacant site, while the eight NN oxygen atoms relax toward the vacancy site, as already noted in Refs. [49,50]. In addition, the TiO_6 octahedra near V_O are subjected to AFD-like rotations [27,43] (see Fig. 3). These structural changes occur irrespective of the polaronic configuration. At the polarons (Ti^{3+}), the lattice relaxes similarly to the Nb-doped case. We emphasize that a proper treatment of local structural relaxations within a large unit cell is of primary importance for achieving a localized solution.

Thus a key element of our results is that the excess electrons induced by V_O do not form a mixed state of free and trapped carriers, as suggested by previous theoretical studies, but rather a "double polaron" with two trapped electrons in distinct Ti^{3+} sites.

Now, how can this scenario explain the temperature-driven MIT observed in $SrTiO_{3-\delta}$ with homogeneously distributed V_Os? To answer this question we have conducted MD runs to probe the possibility to thermally activate the hopping mobility of the V_O-induced small polarons. We have monitored the position of the two polarons as a function of time for different temperatures, each time starting from the ground state configuration P3.

From the $T = 700$ K and $T = 1000$ K results in Fig. 5 we infer that one of the polarons stays bound to the V_O forming a complex [51]. This polaron gives rise to an optical absorption peak at about 1.1 eV below the CBM (see P3 DOS in Fig. 3), whereas the second one can easily hop to other sites, enabling electrical conductivity. This polaron forms a peak at 0.8 eV below the CBM (see P3 DOS in Fig. 3). The oxygen vacancy does not undergo any diffusion during the MD run, in line
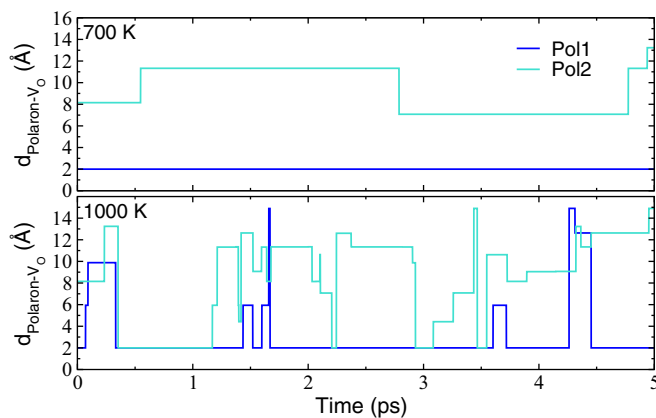
with the reported large migration barrier for oxygen diffusion (0.98 eV) [52].

The mobility increases with increasing temperature. At 1000 K we register 36 polaron migrations in 5 ps. MD finds several other polaron topologies, with many minima close together on the potential energy landscape. The P3 pattern remains the most favorable one ($\approx 65\%$ of the time), followed by P2 ($\approx 20\%$) and P4 ($\approx 10\%$). Importantly, MD never leads to a mixed localized/free-carrier P1-like configuration, although a degree of delocalization naturally emerges in the transition state from one minimum to the next one. The various minima could be populated at finite temperatures. Employing a simple Arrhenius equation, an activation energy of approximately 150 meV is estimated [53].

In order to assess the minimum energy barrier for small polaron hopping, we have investigated an abbreviated version of this process through the climbing image nudged-elastic band method [54], using a $3 \times 3 \times 3$ SC. We obtained migration barriers of 204 meV, 177 meV, and 176 meV for small polaron hopping along the [100], [110], and [111] directions, respectively, in agreement with the value derived from the MD runs.

Our MD results provide a sound interpretation of the temperature-driven MIT in reduced $SrTiO_3$: at high temperature the electrons exhibit hopping mobility, but once the temperature decreases, they will get trapped in polaron levels giving rise to a semiconducting regime [16].

Finally, we would like to mention that we did not find any significant energy difference between the ferromagnetic and antiferromagentic arrangement of the trapped electrons. Hence the hypothesis that V_Os are the cause of the observed ferromagnetism in $SrTiO_3$ [55] deserves further investigation.

IV. SUMMARY

In summary, DFT+U calculations in conjunction with molecular dynamics simulations provide insights into the behavior of excess electrons in $SrTiO_3$. We predict a carrier-density dependent transition between a semiconducting behavior with in-gap polaron states and a conductive regime. Our findings reconcile conflicting experimental data and elucidate the fundamental physics behind. Our account of the oxygen defective $SrTiO_3$ at sufficiently high carrier concentration revisits previous theoretical results and leads to a unified and consistent explanation of the measured data: at low temperature the excess electrons are confined in Ti^{3+} sites and become mobile when thermally activated.

FIG. 5. (Color online) MD in $SrTiO_{3-\delta}$, $\delta = 0.00267$ ($N = 5$). Mobility of the two polarons Pol1 and Pol2 starting from the P3 configuration (see Fig. 3: Pol1 near V_O; Pol2 about 8 Å apart), given with respect to the distance $d_{Pol1/Pol2-V_O}$ between the polaron and V_O for two simulation temperatures, 700 K (top) and 1000 K (bottom). One polaron usually remains in the vicinity of V_O, whereas the other one frequently hops to neighboring sites.

[1] J. F. Schooley, W. R. Hosler, and M. L. Cohen, Phys. Rev. Lett. **12**, 474 (1964).

[2] W. D. Rice, P. Ambwani, M. Bombeck, J. D. Thompson, G. Haugstad, C. Leighton, and S. A. Crooker, Nat. Mater. **13**, 481 (2014).

[3] P. Moetakef, J. R. Williams, D. G. Ouellette, A. P. Kajdos, D. Goldhaber-Gordon, S. J. Allen, and S. Stemmer, Phys. Rev. X **2**, 021014 (2012).

[4] H. Ohta *et al.*, Nat. Mater. **6**, 129 (2007).

[5] D. Kan *et al.*, Nat. Mater. **4**, 816 (2005).

[6] W. Meevasana, P. D. C. King, R. H. He, S-K. Mo, M. Hashimoto, A. Tamai, P. Songsiriritthigul, F. Baumberger, and Z.-X. Shen, Nat. Mater. **10**, 114 (2011).

[7] Z. Wang, Z. Zhong, X. Hao, S. Gerhold, B. Stoeger, M. Schmid, J. Sanchez-Barriga, A. Varykhalov, C. Franchini, K. Held, and U. Diebold, Proc. Natl. Acad. Sci. (U.S.A.) **111**, 3933 (2014).

[8] H. Fröhlich, Adv. Phys. **3**, 325 (1954).

[9] A. S. Alexandrov and J. T. Devreese, in *Devreese Advances in Polaron Physics*, Springer Series in Solid-State Sciences Vol. 159 (Springer-Verlag, New York, 2010).

[10] J. T. Devreese, *Encyclopedia of Applied Physics Vol. 14* (Wiley-VCH Publishers, Inc., New York, 1996), p. 383.

[11] J. L. M. van Mechelen, D. van der Marel, C. Grimaldi, A. B. Kuzmenko, N. P. Armitage, N. Reyren, H. Hagemann, and I. I. Mazin, Phys. Rev. Lett. **100**, 226403 (2008).

[12] J. T. Devreese, S. N. Klimin, J. L. M. van Mechelen, and D. van der Marel, Phys. Rev. B **81**, 125119 (2010).

[13] Y. J. Chang, A. Bostwick, Y. S. Kim, K. Horn, and E. Rotenberg, Phys. Rev. B **81**, 235109 (2010).

[14] T. Kohmoto, D. Ikeda, X. Liang, and T. Moriyasu, Phys. Rev. B **87**, 214301 (2013).

[15] Y. Yamada and Y. Kanemitsu, Phys. Rev. B **82**, 121103(R) (2010).

[16] Z. Q. Liu *et al.*, Phys. Rev. Lett. **107**, 146802 (2011).

[17] Y. Lee, C. Clement, J. Hellerstedt, J. Kinney, L. Kinnischtzke, X. Leng, S. D. Snyder, and A. M. Goldman, Phys. Rev. Lett. **106**, 136809 (2011).

[18] Y. Yamada, H. K. Sato, Y. Hikita, H. Y. Hwang, and Y. Kanemitsu, Phys. Rev. Lett. **111**, 047403 (2013).

[19] Y. Ishida, R. Eguchi, M. Matsunami, K. Horiba, M. Taguchi, A. Chainani, Y. Senba, H. Ohashi, H. Ohta, and S. Shin, Phys. Rev. Lett. **100**, 056401 (2008).

[20] A. Fujimori *et al.*, Phys. Rev. B **46**, 9841 (1992).

[21] T. Higuchi, T. Tsukamoto, K. Kobayashi, Y. Ishiwata, M. Fujisawa, T. Yokoya, S. Yamaguchi, and S. Shin, Phys. Rev. B **61**, 12860 (2000).

[22] M. D'Angelo, R. Yukawa, K. Ozawa, S. Yamamoto, T. Hirahara, S. Hasegawa, M. G. Silly, F. Sirotti, and I. Matsuda, Phys. Rev. Lett. **108**, 116802 (2012).

[23] A. Fujimori *et al.*, J. Phys. Chem. Solids **57**, 1379 (1996).

[24] M. Lee, J. R. Williams, S. Zhang, C. D. Frisbie, and D. Goldhaber-Gordon, Phys. Rev. Lett. **107**, 256601 (2011).

[25] Z. Hou and K. Terakura, J. Phys. Soc. Jpn. **79**, 114704 (2010).

[26] C. Mitra, C. Lin, J. Robertson, and A. A. Demkov, Phys. Rev. B **86**, 155105 (2012).

[27] M. Choi, F. Oba, Y. Kumagai, and I. Tanaka, Adv. Mater. **25**, 86 (2013).

[28] F. El-Mellouhi, E. N. Brothers, M. J. Lucero, and G. E. Scuseria, J. Phys.: Condens. Matter **25**, 135501 (2013).

[29] C. Lin and A. A. Demkov, Phys. Rev. Lett. **111**, 217601 (2013).

[30] A. Janotti, J. B. Varley, M. Choi, and C. G. Van de Walle, Phys. Rev. B **90**, 085202 (2014).

[31] J. P. Perdew, K. Burke, and M. Ernzerhof, Phys. Rev. Lett. **77**, 3865 (1996).

[32] G. Kresse and J. Hafner, Phys. Rev. B **48**, 13115 (1993); G. Kresse and J. Furthmüller, Comput. Mater. Sci. **6**, 15 (1996).

[33] F. Aryasetiawan, K. Karlsson, O. Jepsen, and U. Schönberger, Phys. Rev. B **74**, 125106 (2006).

[34] N. Marzari and D. Vanderbilt, Phys. Rev. B **56**, 12847 (1997).

[35] C. Franchini, R. Kováčik, M. Marsman, S. Sathyanarayana Murthy, J. He, C. Ederer, and G. Kresse, J. Phys.: Condens. Matter **24**, 235602 (2012).

[36] A. A. Mostofi, J. R. Yates, Y.-S. Lee, I. Souza, D. Vanderbilt, and N. Marzari, Comput. Phys. Commun. **178**, 685 (2008).

[37] L. Vaugier, H. Jiang, and S. Biermann, Phys. Rev. B **86**, 165105 (2012).

[38] R. Wahl, D. Vogtenhuber, and G. Kresse, Phys. Rev. B **78**, 104116 (2008).

[39] T. Shibuya, K. Yasuoka, S. Mirbt, and B. Sanyal, J. Phys.: Condens. Matter **24**, 435504 (2012).

[40] N. A. Deskins, R. Rousseau, and M. Dupuis, J. Phys. Chem. C **115**, 7562 (2011).

[41] V. L. Campo, Jr. and M. Cococcioni, J. Phys.: Condens. Matter **22**, 055602 (2010).

[42] G. Makov and M. C. Payne, Phys. Rev. B **51**, 4014 (1995).

[43] K. Uchida, S. Tsuneyuki, and T. Schimizu, Phys. Rev. B **68**, 174107 (2003).

[44] M. Setvin, C. Franchini, X. Hao, M. Schmid, A. Janotti, M. Kaltak, C. G. Van de Walle, G. Kresse, and U. Diebold, Phys. Rev. Lett. **113**, 086402 (2014).

[45] M. Setvin, X. Hao, B. Daniel, J. Pavelec, Z. Novotny, G. Parkinson, M. Schmid, G. Kresse, C. Franchini, and U. Diebold, Ang. Chem., Int. Ed. **53**, 4714 (2014).

[46] J. L. Servoin, Y. Luspin, and F. Gervais, Phys. Rev. B **22**, 5501 (1980).

[47] K. Szot, W. Speier, R. Carius, U. Zastrow, and W. Beyer, Phys. Rev. Lett. **88**, 075508 (2002).

[48] D. A. Muller, N. Nakagawa, A. Ohtomo, J. L. Grazul, and H. Y. Hwang, Nature (London) **430**, 657 (2004).

[49] J. P. Buban, H. Iddir, and S. Öğüt, Phys. Rev. B **69**, 180102 (2004).

[50] J. Carrasco, F. Illas, N. Lopez, E. A. Kotomin, Yu. F. Zhukovskii, R. A. Evarestov, Yu. A. Mastrikov, S. Piskunov, and J. Maier, Phys. Rev. B **73**, 064106 (2006).

[51] A. Janotti, C. Franchini, J. B. Varley, G. Kresse, and C. G. Van de Walle, Phys. Status Solidi RRL **7**, 199 (2013).

[52] A. Yamaji, J. Am. Ceram. Soc. **58**, 152 (1975).

[53] In Ref. [16], an Arrhenius plot of the carrier density is interpreted as an activation energy of 25 meV, but this is for temperatures in the "metallic" conductance regime. In the dopant model suggested there, charge carrier saturation would occur under these conditions; thus the interpretation of the Arrhenius plot is questionable.

[54] G. Henkelman, B. P. Uberuaga, and H. Jónsson, J. Chem. Phys. **113**, 9901 (2000).

[55] Z. Q. Liu *et al.*, Phys. Rev. B **87**, 220405(R) (2013).